Non-stationary transport phenomena in networks of fractures: effective simulations and stochastic analysis

Non-stationary transport phenomena in networks of fractures: effective simulations and stochastic analysis

Stefano Berrone[a,*], Sandra Pieraccini[a], Stefano Scialò[a]

[a]*Dipartimento di Scienze Matematiche, Politecnico di Torino, Corso Duca degli Abruzzi 24, 10129 Torino, Italy.*

Abstract

Among the major challenges in performing underground flow simulations in fractured media are geometrical complexities in the domain and uncertainty in the problem parameters, including the geometrical configuration. The Discrete Fracture Network (DFN) model is largely applied in order to properly account for the directionality of the flow in fractured media. Generation of DFN configurations is usually based on stochastic data and this contributes to generate very complex geometrical configurations for which a conforming mesh generation is often infeasible. Moreover, uncertainty in the geometrical and hydro-geological properties calls for a deep uncertainty quantification analysis; the corresponding huge computational cost of the simulations requires modern efficient approaches faster and cheaper than the classical Monte Carlo approach. In this paper we numerically investigate both these aspects, proposing a viable solution for dealing with geometrical complexities arising in the computation of the hydraulic head and in the solution of the unsteady transport problem of a passive scalar in the DFN, and for dealing with uncertainties in hydro-geological parameters of the fracture distribution considered.

Keywords: Fracture flows, Darcy flows, discrete fracture networks, optimization methods for elliptic problems, uncoupled large scale simulations, XFEM, advection-diffusion in DFNs, unsteady flow in DFNs
2010 MSC: 65N30, 65N50, 68U20, 86-08

*Corresponding author
Email addresses: stefano.berrone@polito.it (Stefano Berrone), sandra.pieraccini@polito.it (Sandra Pieraccini), stefano.scialo@polito.it (Stefano Scialò)

1. Introduction

Simulation of transport phenomena in underground fractured media is a key issue in many applications requiring the analysis of the advection-diffusion transport of a passive pollutant immersed in a bulk fluid, such as aquifers monitoring, disposal and geological storage of nuclear wastes, and, more in general, the control of the dispersion in the subsoil of any kind of contaminant deriving from industrial activities.

According to the Discrete Fracture Network (DFN) model [1, 2, 3, 4, 5, 6, 7], the underground is described as a rock matrix crossed by a network of intersecting fractures, each one being modeled as a planar polygon; fracture-resembling polygons intersect each other in segments called *traces* (see Figure 1). DFN models are an alternative to continuum-like models [8], for geological sites with a relatively low density of fractures, and are particularly useful for the description of transport phenomena, as they allow for a realistic representation of the directionality of the flow. Dimensions, orientation and hydraulic properties of the fractures in a DFN are extrapolated by probability distribution functions, derived from experimental data and samplings of the ground.

As a consequence of the stochastic generation of the networks, DFNs for practical applications are usually intricate networks, counting a large number of fractures and fracture intersections, with possibly critical features such as, for examples, very narrow angles formed by intersecting traces, non intersecting traces very close to each other and traces with length spanning several orders of magnitude. These geometrical complexities require targeted approaches for the discretization of the governing system of equations , moving from standard finite elements on conforming meshes to more unconventional settings [9, 10, 11, 12, 13, 14, 15]. In fact, it is well known that the generation of a mesh conforming to fracture intersections in a DFN often results in an infeasible process, due to the extremely large number of constraints, or would yield poor quality meshes, which in practice could not be used. Due to the above mentioned complexities, the simulation of transient flows and transport phenomena in discrete fracture networks is still a very challenging task. Some recent works on the subject can be found in [16, 17, 18, 19, 20].

In the present work, we will focus on the effective simulations of unsteady advection-diffusion processes in DFNs by means of a reformulation of the problem as a PDE-constrained optimization problem. We propose a modification of the optimization-based approach introduced in [13, 21, 22] and further developed in [23, 24, 25, 26, 27, 28]; this new formulation is suitable for the application in the advection-diffusion framework in DFNs. The approach inherits the advantages of the original optimization approach:

namely, the meshing process can be performed independently on each fracture; this makes the method a reliable and robust resolution tool, with an intrinsic parallel nature. These characteristics are of paramount importance also to perform uncertainty quantification analyses of transport phenomena.

The starting point of the new approach is the computation of the Darcy velocity in the DFN, which is a function of the gradient of the hydraulic head. The evaluation of the hydraulic head is performed by means of the optimization approach [13, 21, 22], in which the matching conditions prescribing continuity of the hydraulic head and flux balance at fracture intersections are imposed through the minimization of a proper functional, and the equations for the Darcy law on the fractures act as constraints for the minimization process. Conditions of continuity of the hydraulic head and flux balance at fracture intersection are a common choice in DFN flow simulations [9, 29], but alternative choices prescribing more complex matching conditions (see, e.g., [30, 31, 19]) could be plugged in the optimization framework. The computed velocity field is then post-processed to remove the small components of the computed velocity in the direction normal to the fracture boundaries due to the numerical approximation of the solution where a no-flow boundary condition is prescribed. Then, the unsteady advection-diffusion problem is tackled again with a PDE-constrained optimization approach with modified constraints to account for the transport problem and for the SUPG-stabilization terms for advection-dominated flow regimes [32].

Furthermore, due to the stochastic generation of the network features, an uncertainty quantification analysis of the output of the simulations, as a function of the random parameters affecting the network, is of crucial importance. Here, we will focus on a framework in which the hydro-geological properties of the fractures are stochastically generated, whereas the geometry is assumed to be deterministic. We will use effective, recently developed uncertainty quantification techniques to analyse the effect of a stochastic transmissivity, with a prescribed distribution, on the transport of pollutants in DFNs in a time dependent framework. The use of a stochastic collocation approach on sparse grids allows to perform an uncertainty quantification analysis with a number of simulations which is smaller than the one required by, e.g., Monte Carlo method. Keeping the number of simulations as small as possible is a crucial issue, considering the high computational cost of each time-dependent simulation in large DFNs.

The structure of the paper is as follows. In Section 2 we introduce some useful notation; in Section 3 we describe the problem providing the transport velocity field, whereas in Section 4 we introduce the advection-diffusion formulation of the problem, followed by the discrete formulation in Section 5; Section 6 is devoted to the introduction of the uncertainty quantification

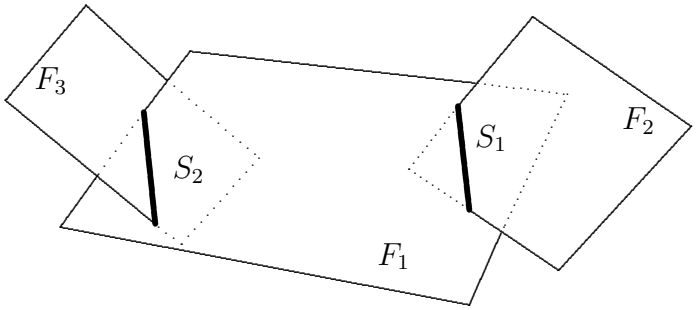

Figure 1: Example of network

setting. Finally, numerical results are proposed and discussed in Section 7.

2. Definitions and main assumptions

Let $\mathcal{D}$ denote the DFN, given by the union of planar polygonal fractures F_i, $i = 1, \dots, I$, intersecting each other to form traces; let S_m, $m = 1, \dots, M$, be the traces; see Figure 1. Let $\mathcal{S}$ denote the set of all traces in $\mathcal{D}$, whereas $\mathcal{S}_i$ is the set of the traces on F_i. We assume that the overall set $\mathcal{D}$ is connected. We also assume that each trace S_m is given by the intersection of two fractures, say $S_m = F_i \cap F_j$; the link between the trace S_m and the couple of intersecting fractures will be highlighted by introducing the following notation: $I_{S_m} := \{i, j\}$.

In the present context we will consider the rock matrix surrounding fractures as impervious, so that flow can only occur through the fracture planes and in the normal direction across the traces. Given a function $\zeta \in \mathrm{H}^1(F_i)$, $\forall i$, and a uniformly positive definite tensor function $\mathbf{q}$, the symbol $\left[\!\left[(\mathbf{q}\nabla\zeta)\cdot n^i_{S_m}\right]\!\right]_{S_m}$ denotes the jump of the co-normal derivative of ζ across trace S_m, being $n^i_{S_m}$ the unit vector with a fixed direction normal to trace S_m on F_i. The symbol $\|\cdot\|_{\alpha,\vartheta}$ will denote a norm in the Sobolev space $\mathrm{H}^\alpha(\vartheta)$; sometimes, for the sake of increasing clarity, the functional space will be explicitly denoted with a subscript.

The boundary of $\mathcal{D}$, $\partial\mathcal{D}$, is split into a Dirichlet part, $\Gamma^D \neq \emptyset$, and a Neumann part, Γ^N, such that $\partial\mathcal{D} = \Gamma^D \cup \Gamma^N$ and $\Gamma^D \cap \Gamma^N = \emptyset$. The boundary of each fracture ∂F_i is split accordingly in a Dirichlet part $\Gamma^D_i = \partial F_i \cap \Gamma^D$ and a Neumann part $\Gamma^N_i = \partial F_i \cap \Gamma^N$. Functions G^D and G^N prescribe boundary conditions on Γ^D and Γ^N, respectively, whereas G^D_i and G^N_i are the corresponding restrictions to Γ^D_i and Γ^N_i. We then introduce the functional

spaces

$$V_i^D = \mathrm{H}^1_{\mathrm{D}}(F_i) = \left\{ v \in \mathrm{H}^1(F_i) : v_{|\Gamma_i^D} = G_i^D \right\},$$
$$V_i = \mathrm{H}^1_{0,\mathrm{D}}(F_i) = \left\{ v \in \mathrm{H}^1(F_i) : v_{|\Gamma_i^D} = 0 \right\},$$

and the dual space $(V_i)'$. Given a positive time T, we also introduce the space

$$\mathcal{W}_i = \left\{ w : \int_0^T \|w(t)\|^2_{V_i} \, \mathrm{d}t < \infty \text{ and } \int_0^T \|\frac{\partial w}{\partial t}\|^2_{(V_i)'} \, \mathrm{d}t < \infty \right\}. \tag{1}$$

In order to solve the advection-diffusion problem of a passive pollutant in a DFN $\mathcal{D}$ we are first interested in determining the Darcy velocity. In the following, a hat symbol ($\widehat{\ }$) will be used in order to denote quantities related to the Darcy velocity problem; for example, $\widehat{\Gamma}^D$ represents the Dirichlet boundary for the Darcy velocity problem, whereas Γ^D represents the Dirichlet boundary in the advection-diffusion problem.

3. The Darcy velocity problem

The hydraulic head H is defined by $H = \mathcal{P} + \zeta$, where ζ is the elevation and $\mathcal{P} = p/\rho g$, being p the fluid pressure, g the gravitational acceleration and ρ the fluid density. The hydraulic head is governed by the Darcy law on each fracture of the DFN $\mathcal{D}$, and is a continuous function across the traces with discontinuous first order derivatives. On each fracture, the jump of the gradient of the hydraulic head in the direction normal to a trace corresponds to the flux leaving or entering the fracture through the trace itself, and it is balanced by the flux jump on the other intersecting fracture. Starting from H it is possible to compute the Darcy velocity β in $\mathcal{D}$. Let us assume to split the fractures in the DFN into sub-fractures (i.e., portion of fractures cut along the traces, thus without internal traces, [13]), such that each trace is now part of the boundary of some of the new sub-fractures. Assuming that there are no sources or sinks of hydraulic head in the sub-fractures, the DFN problem on the new sub-fractures f_k is written as: for all $k = 1, \ldots, I_f$

$$\begin{cases} -\nabla \cdot (\mathbf{K}_{f_k} \nabla H) &= 0 & \text{in } f_k, \\ H_{|\widehat{\Gamma}^D \cap \partial f_k} &= \widehat{G}^D & \text{on } \widehat{\Gamma}^D \cap \partial f_k, \\ (\mathbf{K}_{f_k} \nabla H) \cdot n_{\widehat{\Gamma}^N \cap \partial f_k} &= \widehat{G}^N & \text{on } \widehat{\Gamma}^N \cap \partial f_k, \end{cases} \tag{2}$$

where $\mathbf{K}_{f_k}$ is a uniformly positive definite tensor function representing the transmissivity of the sub-fracture f_k and $n_{\widehat{\Gamma}^N \cap \partial f_k}$ is the outward unit vector

normal to the boundary of f_k. The previous equations are completed with the following additional constraints: $\forall m = 1, \ldots, M$ and $k, p = 1, \ldots, I_f$ such that $\partial f_k \cap S_m \neq \emptyset$ and $\partial f_p \cap S_m \neq \emptyset$

$$H_{|\partial f_k \cap S_m} = H_{|\partial f_p \cap S_m}, \tag{3}$$

$$\sum_{k=1,..,I_f \ : \ \partial f_k \cap S_m \neq \emptyset} (\mathbf{K}_{f_k} \nabla H) \cdot n_{\partial f_k \cap S_m} = 0. \tag{4}$$

If we define $\beta \in \mathrm{H}^{\mathrm{div}}(F_i)$ such that $\beta_{|f_k} = -\mathbf{K}_{f_k} \nabla H$, then, according to the previous setting we have $\nabla \cdot \beta_{|f_k} = 0$, and β is such that there is mass conservation across each trace of the DFN. We remark that, in the present work, the hydraulic head distribution in $\mathcal{D}$ is not computed solving equations (2)-(4), but following the optimization approach proposed in [13, 21, 22] and further developments. According to the framework proposed in these references, the problem previously written on the sub-fractures can be stated on the whole fractures F_i, introducing, on each trace, additional unknowns $\widehat{U}_i^m = \widehat{\alpha} H_{i|S_m} + \left[\!\left[(\mathbf{K} \nabla H_i) \cdot n^i_{S_m} \right]\!\right]_{S_m}$, in which $\widehat{\alpha}$ is a positive parameter. The problem is stated as follows: $\forall i = 1, \ldots, I$, find $H_i \in \widehat{V}_i^D$ such that: $\forall v \in \widehat{V}_i$

$$\int_{F_i} \mathbf{K} \nabla H_i \nabla v \mathrm{d}\mathcal{D} + \widehat{\alpha} \sum_{S_m \in \mathcal{S}_i} \int_{S_m} H_{i|S_m} v_{|S_m} = \sum_{S_m \in \mathcal{S}_i} \left\langle \widehat{U}_i^m, v_{|S_m} \right\rangle_{\mathrm{H}^{-\frac{1}{2}}(S_m), \mathrm{H}^{\frac{1}{2}}(S_m)}.$$

The previous equations are completed by the additional constraints: $\forall m = 1, \ldots, M$ and for $i, j \in I_{S_m}$

$$H_{i|S_m} - H_{j|S_m} = 0, \tag{5}$$

$$\left[\!\left[(\mathbf{K} \nabla H_i) \cdot n^i_{S_m} \right]\!\right]_{S_m} + \left[\!\left[(\mathbf{K} \nabla H_j) \cdot n^j_{S_m} \right]\!\right]_{S_m} = 0. \tag{6}$$

This problem is solved enforcing the coupling conditions (5)-(6) by a PDE-constrained optimization method. In the next Section, we will describe this optimization method in a new formulation which takes into account non-stationary solutions and transport phenomena.

4. Advection-diffusion problem formulation

Let us now state the formulation of the advection-diffusion problem in a network of fractures. Let us denote by $\mathcal{C}$ the function expressing the concentration of a passive scalar in $[0, T] \times \mathcal{D}$, and by $\mathcal{C}_i$ its restriction to fracture F_i. Then, let us denote by $(\cdot, \cdot)_\vartheta$ the $\mathrm{L}^2(\vartheta)$-scalar product, and let us introduce the symmetric bilinear form $a_i : V_i \times V_i \mapsto \mathbb{R}$:

$$a_i(u, v) = \int_{F_i} \mu_i \nabla u \nabla v \, \mathrm{d}\mathcal{D} + \alpha \sum_{S_m \in \mathcal{S}_i} \int_{S_m} u_{|S_m} v_{|S_m} \mathrm{d}s,$$

in which μ_i is the diffusivity of the pollutant in the bulk fluid on F_i and $\alpha > 0$ is a constant scalar parameter; finally, the bilinear form $b_i : V_i \times V_i \mapsto \mathbb{R}$ is set as

$$b_i(u, v) = \int_{F_i} \beta_i \cdot \nabla u v \, \mathrm{d}\mathcal{D},$$

where β_i is the restriction of the Darcy velocity β to F_i. Furthermore, let $\mathcal{C}_{i,0} \in \mathrm{L}^2(F_i)$ be the initial condition for the concentration $\mathcal{C}_i$.

With these definitions at hand, the problem of interest can be stated as follows: $\forall i = 1, \ldots, I$ find $\mathcal{C}_i \in \mathcal{W}_i$, satisfying $\mathcal{C}_i(0, \cdot) = \mathcal{C}_{i,0}$, such that, $\forall v_i \in V_i$,

$$\frac{\mathrm{d}}{\mathrm{d}t}(\mathcal{C}_i, v_i)_{F_i} + a_i(\mathcal{C}_i, v_i) + b_i(\mathcal{C}_i, v_i) = \sum_{S_m \in \mathcal{S}_i} \left\langle U_i^m, v_{i|S_m} \right\rangle_{\mathrm{H}^{-\frac{1}{2}}(S_m), \mathrm{H}^{\frac{1}{2}}(S_m)}, \quad (7)$$

with the following additional conditions: $\forall m = 1, \ldots, M$ and for $i, j \in I_{S_m}$

$$\mathcal{C}_{i|S_m} - \mathcal{C}_{j|S_m} = 0, \quad (8)$$

$$\left[\!\left[(\mu_i \nabla \mathcal{C}_i) \cdot n^i_{S_m}\right]\!\right]_{S_m} + \left[\!\left[(\mu_j \nabla \mathcal{C}_j) \cdot n^j_{S_m}\right]\!\right]_{S_m} = 0, \quad (9)$$

a.e. in $(0, T)$. In the previous equations we have set

$$U_i^m = \left[\!\left[(\mu_i \nabla \mathcal{C}_i) \cdot n^i_{S_m}\right]\!\right]_{S_m} + \alpha \, \mathcal{C}_{i|S_m}$$

and we have neglected any forcing function, for simplicity of notation. Conditions (8)-(9) express the continuity of the concentration of the pollutant across the traces at each time-frame and the balance of the diffusive flux across the traces. We finally observe that the advective flow is balanced across the traces, according to the definition of β.

In order to introduce an alternative formulation for the matching conditions at the interfaces (i.e., at the traces) we introduce the following cost functional:

$$J(\mathcal{C}, U) = \frac{1}{2} \sum_{i=1}^{I} \sum_{m=1}^{M} \left\| \mathcal{C}_{i|S_m} - \mathcal{C}_{j|S_m} \right\|^2_{\frac{1}{2}, S_m} + \left\| U_i^m + U_j^m - \alpha \left(\mathcal{C}_{i|S_m} + \mathcal{C}_{j|S_m} \right) \right\|^2_{-\frac{1}{2}, S_m}, \quad (10)$$

where for all $m = 1, \ldots, M$, indexes i, j are taken in I_{S_m}.

The functional J is quadratic, and it can be proven, following the arguments of [13], that for each fixed time t it has a unique minimum if it is minimized constrained by (7). The optimization formulation of the advection-diffusion problem in a network of fractures is then: for each $t \in [0, T]$

$$\begin{aligned} &\min J(\mathcal{C}, U) \\ &\text{subject to (7) for } i = 1, \ldots, I, \end{aligned} \quad (11)$$

in which the functions U_i^m act as control variables, with $U_i^m \in \mathrm{H}^{-\frac{1}{2}}(S_m)$ a.e. in $(0,T)$.

5. Discrete formulation

As already mentioned, the advantages of the optimization approach for the advection-diffusion problems in DFNs are the flexibility and the robustness of the method, as outcomes of the possibility of an independent meshing process on each fracture of the DFN, not conforming to fracture intersections. Good quality meshes are easily generated, indeed, and the non-conformities at fracture intersections are handled through the cost functional. Furthermore, when problem size becomes an issue, the optimization approach allows for a natural parallel implementation, splitting the original high-dimension problem into smaller sub-problems on the fractures. We refer the reader to [26] for further details.

Let us now sketch the discrete formulation of the advection-diffusion problem in DFNs. To this end, let us introduce on each fracture F_i a triangulation $\mathcal{T}_{i,\delta}$, independently generated from those on the other fractures, suitable for a finite element based discretization. On each triangulation we build the finite dimensional subspace V_i^δ of the functional space V_i, $i = 1, \ldots, I$, with dimension N_i, and we set $N^F = \sum_{i=1}^I N_i$. For each trace S_m, $m = 1, \ldots, M$, and for each of the two fractures F_ℓ with $\ell \in I_{S_m}$, we build an independent space discretization and introduce a finite dimensional space $\mathcal{U}_\ell^{m,\delta} \subset \mathrm{L}^2(S_m) \subset \mathrm{H}^{-\frac{1}{2}}(S_m)$ with dimension N_ℓ^m. We set $N^S = \sum_{i=1}^I \sum_{S_m \in \mathcal{S}_i} N_i^m$. The discrete approximation, on each fracture, of $\mathcal{C}_i$ is $c_i = \sum_{k=1}^{N_i} c_{i,k}\varphi_{i,k}$, whereas the discrete counterpart of the control variable U_i^m is $u_i^m = \sum_{k=1}^{N_i^m} u_{i,k}^m \psi_{i,k}$. The norms involved in the definition of the discrete functional are computed in L^2, and thus the discrete functional is written as:

$$J(c,u) = \frac{1}{2} \sum_{i=1}^{I} \sum_{m=1}^{M} \left\| c_{i|S_m} - c_{j|S_m} \right\|_{0,S_m}^2 + \left\| u_i^m + u_j^m - \alpha \left(c_{i|S_m} + c_{j|S_m} \right) \right\|_{0,S_m}^2 .$$

Let us now introduce, on each fracture F_i, the Péclet non-dimensional number $\mathrm{Pe}_i = \frac{\|\beta_i\| L_i}{2\mu_i}$, in which L_i is a characteristic dimension of fracture F_i, and, for each element $E \in \mathcal{T}_{i,\delta}$ the element Péclet number $\mathrm{Pe}_{i,E} = m_{i,E} \frac{\|\beta_{i|E}\| \delta_E}{2\mu_{i|E}}$, where δ_E is the diameter of E and $m_{i,E}$ is defined as in [33], i.e., $m_{i,E} = \min\{\frac{1}{3}, 2C_E\}$, being C_E an estimate of the largest constant satisfying the inverse inequality [34]

$$C_E \sum_{E \in \mathcal{T}_{i,\delta}} \delta_E^2 \|\Delta\varphi\|_{0,E}^2 \leq \|\nabla\varphi\|_{0,F_i}^2, \quad \forall \varphi \in V_i^\delta.$$

We then define the parameter $\tau_{i,E}$ as

$$\tau_{i,E} = \frac{\delta_E}{2\|\beta_{i|E}\|} \min(\mathrm{Pe}_{i,E}, 1).$$

Approximating the time derivative by the Implicit Euler method with $\Delta t = t^{[n+1]} - t^{[n]}$, and recalling that we have no forcing function, the discrete problem formulation is: for $n = 0, 1, \ldots,$ solve

$$\begin{aligned}
&\min J(c^{[n+1]}, u^{[n+1]}) \\
&\text{subject to, for } i = 1, \ldots, I, \forall k = 1, \ldots, N_i \\
&\frac{1}{\Delta t}(c_i^{[n+1]}, \varphi_{i,k})_{F_i} + a_i(c_i^{[n+1]}, \varphi_{i,k}) + b_i(c_i^{[n+1]}, \varphi_{i,k}) + \\
&\sum_{E \in \mathcal{T}_{i,\delta}} (R_i^{[n+1]}, \tilde{\tau}_{i,E} \beta_{i|E} \nabla \varphi_{i,k})_E = \sum_{S_m \in \mathcal{S}_i} \big((u_i^m)^{[n+1]}, \varphi_{i,k|_{S_m}}\big) + \frac{1}{\Delta t}(c_i^{[n]}, \varphi_{i,k})_{F_i} \quad (12)
\end{aligned}$$

in which the last term on the left-hand side accounts for SUPG stabilization [33] for advection dominated flow regimes, being

$$R_i^{[n+1]} = \frac{c_i^{[n+1]} - c_i^{[n]}}{\Delta t} + \nabla \cdot (\mu_i \nabla c_i^{[n+1]}) + \beta_i \cdot \nabla c_i^{[n+1]},$$

and, see for example [35],

$$\frac{1}{\tilde{\tau}_{i,E}} = \frac{1}{\Delta t} + \frac{1}{\tau_{i,E}}.$$

6. Uncertainty quantification techniques

In this section we describe the techniques used in order to perform the uncertainty quantification on the outputs of the simulations. We consider herein a DFN described by deterministic geometric parameters (such as fracture dimensions, positions, orientations...), boundary data and source terms. On the contrary, the transmissivity is assumed to be a random variable, endowed with a certain probability distribution. The solution $(\mathcal{C}, U)$ is therefore seen as a dependent random variable, of which we are interested in computing suitable statistics. For easing the notation, we will avoid in this section the explicit reference to the dependency of $\mathcal{C}$ and U on $(t, \mathbf{x})$. We start briefly describing the uncertainty quantification setting, by closely following [25]. In Section 7 we will detail the specific application considered herein.

Let $(\Omega, \mathcal{F}, \mathbb{P})$ denote a complete probability space, where Ω is the set of outcomes, $\mathcal{F}$ a σ-algebra, and $\mathbb{P} : \Omega \to [0, 1]$ the probability measure.

Let $D \subset \mathbb{R}^d$, $d \leq 3$, be a bounded Lipschitz domain. In a realistic network composed by a large number of fractures, it is unlikely that the set of fracture transmissivities are represented by a collection of independent, or even uncorrelated, random variables. We rather consider a *stochastic field* for describing the fracture transmissivities: namely, we consider a function $K(\mathbf{x}, \omega) : \bar{D} \times \Omega \to \mathbb{R}$ such that, for each fixed point $\mathbf{x} \in D$, the quantity $K(\mathbf{x}, \cdot)$ is a random variable representing the transmissivity at point $\mathbf{x} \in D$. The stochastic field may be approximated by a finite (possibly small) number of stochastic variables following, e.g., the Karhunen-Loéve expansion approach (see, for example, [36] and references therein). Following this approach, the stochastic field is represented as an (infinite) sum of terms obtained from a spectral decomposition of its correlation function; by making a suitable truncation of the expansion, we may describe the stochastic feature of the medium by means of a moderate number of stochastic variables. We briefly sketch in the following this approach, while referring the reader to [25] for more details.

Let us introduce $\kappa = \log_b K$, being $b > 1$ a fixed constant; indeed, since in realistic applications the fracture transmissivities typically span several orders of magnitude, the analysis is preferably performed in terms of the logarithm of the transmissivity. Let us assume that the auto-covariance function $C_\kappa(\mathbf{x}, \mathbf{z})$ of κ, i.e., the function

$$C_\kappa(\mathbf{x}, \mathbf{z}) = \mathbb{E}[(\kappa(\mathbf{x}, \cdot) - \mathbb{E}[\kappa](\mathbf{x}))(\kappa(\mathbf{z}, \cdot) - \mathbb{E}[\kappa](\mathbf{z}))], \qquad \mathbf{x}, \mathbf{z} \in D,$$

is a known continuous function on $D \times D$. We consider the Karhunen-Loève decomposition of κ

$$\kappa(\mathbf{x}, \omega) = \mathbb{E}[\kappa](\mathbf{x}) + \sum_{n=1}^{\infty} \sqrt{\lambda_n} \varphi_n(\mathbf{x}) Y_n(\omega) \ , \tag{13}$$

where $\varphi_n(\mathbf{x})$, $n \geq 1$, are the orthonormal eigenfunctions (with corresponding positive eigenvalues λ_n) of the compact operator $T\varphi = \int_D C_\kappa(\cdot, \mathbf{z})\varphi(\mathbf{z})\mathrm{d}\mathbf{z}$. We recall that the eigenvalues are in non-increasing order, and Y_n are mutually uncorrelated random variables satisfying $\mathbb{E}[Y_n] = 0$, $\mathbb{E}[Y_n^2] = 1$. As it is clear from equation (13), each term of the expansion is given by a deterministic function $\varphi_n(\mathbf{x})$ times a random variable $Y_n(\omega)$; these random variables have in charge the stochastic behaviour of κ and their distribution function is therefore related to the stochastic behaviour of κ. If, for example, κ is a Gaussian process, the random variables Y_n have normal distribution.

By truncating the expansion after the first N terms, for some $N \geq 1$, we

approximate $\kappa(\mathbf{x},\omega)$ by the quantity

$$\kappa_N(\mathbf{x},\omega) = \mathbb{E}[\kappa](\mathbf{x}) + \sum_{n=1}^{N} \sqrt{\lambda_n}\varphi_n(\mathbf{x})Y_n(\omega) \ , \tag{14}$$

which depends on a finite number N of stochastic variables, the truncation parameter N therefore representing the stochastic dimension. Clearly, the higher is the stochastic dimension, the better is the approximation of the stochastic field, but the more complex are the computations involving the stochastic variables. The number of terms to be retained for a good approximation clearly depends on the rate of decay of the eigenvalues, which in turn depends on the smoothness of the correlation kernel $C_\kappa(\mathbf{x},\mathbf{z})$ and on the correlation length.

For a fixed value of the stochastic dimension N, the transmissivity $K_{i,N}$ on each fracture is finally obtained from κ_N as follows: we set $K_{i,N}(\omega) = K_N(\mathbf{x}_i,\omega)$ where $\mathbf{x}_i$ is the position of the center of mass of the fracture and

$$K_N(\mathbf{x},\omega) = b^{\kappa_N(\mathbf{x},\omega)}.$$

Note that for the sake of simplicity the transmissivity $K_{i,N}$ is assumed here to be constant on each fracture, the quantity κ_N being computed at the center of mass of F_i. Nonetheless, the same framework can be applied retaining, in K_N and κ_N, the dependence on the space variable $\mathbf{x}$, thus considering a transmissivity on each fracture which depends on the local coordinate system on F_i.

The solution to the problem is therefore described by a finite set of random variables: $(\mathcal{C}(\omega), U(\omega)) = (\mathcal{C}(Y_1(\omega),\dots,Y_N(\omega)), U(Y_1(\omega),\dots,Y_N(\omega)))$. Let

$$\Phi(\omega) := \Phi(\mathcal{C}(\omega), U(\omega)) = \hat{\Phi}(Y_1(\omega),\dots,Y_N(\omega))$$

denote the quantity of interest. In several applications related to DFNs, Φ represents, for example, the overall flux flowing through the network. The interest is in computing statistics of Φ, namely, mean value (expectation) and variance

$$\mathbb{E}(\Phi) = \int_\Omega \Phi(\omega)\,\mathrm{d}\mathbb{P} \ , \qquad\qquad \sigma^2(\Phi) = \mathbb{E}(\Phi^2) - \mathbb{E}(\Phi)^2 \ ,$$

provided Φ has bounded second-order moment (i.e., $\Phi \in L^2(\Omega,\mathrm{d}\mathbb{P})$). Let us denote by Γ_n the image of Y_n (namely, $\Gamma_n = Y_n(\Omega)$), with $\Gamma = \prod_{n=1}^{N}\Gamma_n$; let $\rho : \Gamma \to \mathbb{R}^+$ be the joint probability function of $Y_1,\dots,Y_n$. Then, the mean value of Φ is computed as

$$\mathbb{E}(\Phi) = \int_{\Gamma} \Phi(y_1, \ldots, y_n)\rho(y_1, \ldots, y_n)\mathrm{d}y_1 \ldots \mathrm{d}y_N.$$

In order to efficiently compute accurate approximations of the statistics of interest, we adopt a stochastic collocation approach (see, e.g., [37, 38, 39]). Within this approach, the problem is solved at suitably – and deterministically – selected points chosen in Γ (the *collocation points*) and then the statistics of interest are computed through numerical integration with proper quadrature formulas built on the collocation points. The stochastic collocation approach allows therefore for a *non-intrusive* implementation in which the deterministic solver is used as a black-box, and the model equations are solved several times with different input data corresponding to the collocation points.

A wise choice of the collocation points in Γ is fundamental for the overall efficiency, in particular when the stochastic dimension N increases, as the computational cost of a full tensorization of 1D grids would be prohibitive. A widely used remedy consists in resorting to *sparse grids* [40, 41], in which only suitable subsets of tensorial grids are used. As far as the univariate quadrature formulas are concerned, the use of high-precision nested grids is worthwhile. Indeed, if – for a fixed stochastic dimension N – the stochastic mesh has to be refined in order to improve the accuracy in the computations of the statistics of Φ, information from the coarser mesh can be re-used. For the uniform probability density, one can use Gauss-Patterson formulas [42] or Clenshaw-Curtis formulas [43]. For the normal probability density, Kronrod-Patterson-Normal (KPN) formulas [44] are a possible choice. Multidimensional sparse quadrature formulas are then built according, e.g., to Smolyak's recipe [40].

7. Numerical results

In this section we propose some numerical tests: first, a simple DFN configuration is considered with simulations tailored at showing optimal convergence properties of the method. Then a more complex DFN is tackled, performing an uncertainty quantification analysis following the lines depicted in Section 6, aimed at assessing the effects of a random fracture transmissivity on the dispersion of a pollutant in the subsoil. Numerical results are obtained using first order extended finite elements (XFEM) [45] on triangular non-conforming meshes. Optimization problems are written in saddle point formulation, [21]; given the moderate size of the considered problems, a direct solver is used to solve the linear systems. The mesh parameter is denoted by δ and represents the maximum element area.

7.1. Validation tests

As a first example, labelled PV, let us consider a DFN $\mathcal{D}$ composed of two rectangular fractures F_1 and F_2 intersecting in the 3D space along a trace S, as shown in Figure 2, left. With reference to the coordinate system $Oxyz$ reported in the figure, let us introduce the following function on $\mathcal{D}$:

$$\mathcal{C} = \begin{cases} (1 - \mathrm{e}^{-t}) \left(y(y-1)|x|(x^2-1) \right), & \text{in } F_1, \\ (1 - \mathrm{e}^{-t}) \left(y(1-y)|z|(z^2-1) \right), & \text{in } F_2. \end{cases} \tag{15}$$

Consider the following problem defined on $\mathcal{D}$: find $\mathcal{C}_i \in \mathcal{W}_i$, $i = 1, 2$, such that a.e. in $(0, 1)$

$$\frac{\mathrm{d}}{\mathrm{d}t}(\mathcal{C}_i, v_i)_{F_i} + a_i(\mathcal{C}_i, v_i) + b_i(\mathcal{C}_i, v_i) = \left\langle U_i^1, v_{i|S} \right\rangle_{\mathrm{H}^{-\frac{1}{2}}(S), \mathrm{H}^{\frac{1}{2}}(S)} + (q_i, v_i), \quad \forall v_i \in V_i, \tag{16}$$

with additional constraints (8)-(9), initial condition $\mathcal{C}(0, \cdot) = 0$ and homogeneous Dirichlet boundary conditions on $\partial\mathcal{D}$. In the previous equation $q_i \in \mathrm{L}^2(F_i)$ is a load term computed in such a way that $\mathcal{C}$ given by (15) is the exact solution. The velocity field β is defined on each fracture as follows:

$$\beta_1 = \begin{cases} (1,0,0) & x < 0, \\ (0,0,0) & x \geq 0, \end{cases} \qquad \beta_2 = \begin{cases} (0,0,-1) & z < 0, \\ (0,0,0) & z \geq 0. \end{cases}$$

The velocity field, thus, has a jump across S on each of the fractures, but is preserving mass conservation on the whole $\mathcal{D}$. Diffusivity of the pollutant in the bulk fluid is $\mu = 10^{-6}$.

7.1.1. Stationary solution

A convergence analysis with respect to the space variables is proposed, considering the steady state solution of PV. The space mesh parameter varies from $\delta = 10^{-1}$ to $\delta = 10^{-4}$, thus resulting in a maximum grid Péclet number ranging from about 6.5×10^4 on the coarsest mesh to 3×10^3 on the finest mesh. The numerical solution on an intermediate mesh ($\delta = 5 \times 10^{-2}$) is shown in Figure 2, right, whereas convergence curves of the error in the H^1 and L^2 norms against mesh refinement are reported in Figure 3, left, showing asymptotic optimal trends.

7.1.2. Transient solution

Convergence with respect to the time discretization parameter Δt is also analyzed. Tests are performed on the finest spatial grid with values of Δt ranging from 0.25 to 3.125×10^{-2}. The expected linear decreasing trend of

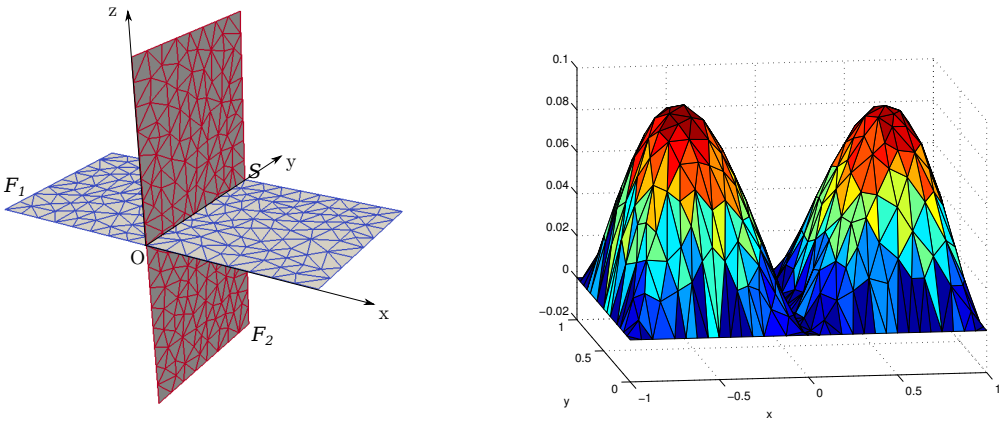

Figure 2: Test PV. Left: computational domain and non-conforming mesh, $\delta = 5 \times 10^{-2}$. Right: numerical solution of the stationary problem on F_1, $\delta = 5 \times 10^{-2}$

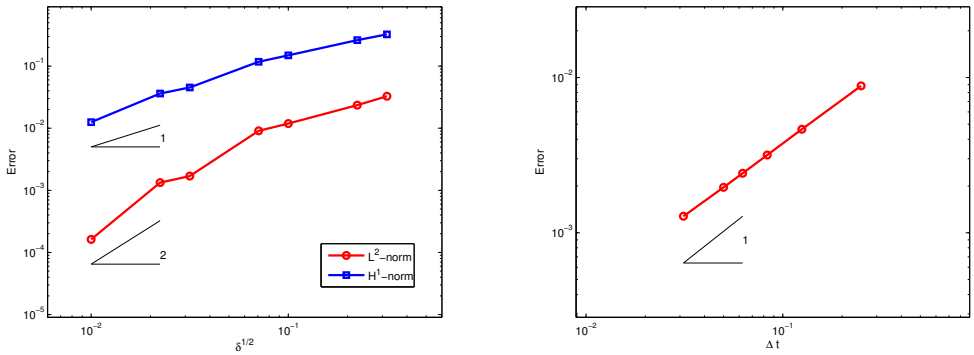

Figure 3: Test PV. Convergence curves versus spatial mesh refinement (left) and versus refinement in time grid (right)

the error is obtained, measured in the L^2-norm in space and L^∞-norm in time. The results are reported in Figure 3. For smaller values of Δt a progressive degradation of the convergence trend is observed, due to the effect of space discretization errors.

7.2. A dispersion problem with uncertain transmissivity

The second numerical experiment, labelled P_{uq}, tackles the issue of randomness of input data for DFN simulations, combining the proposed optimization approach for the flow and transport simulation with the aforementioned uncertainty quantification strategies. With this example we aim at proving the viability of the proposed approaches in realistic situations.

We consider a scenario in which, over a large fault, the rock matrix is crossed by a network of fractures, forming a DFN composed of 24 fractures

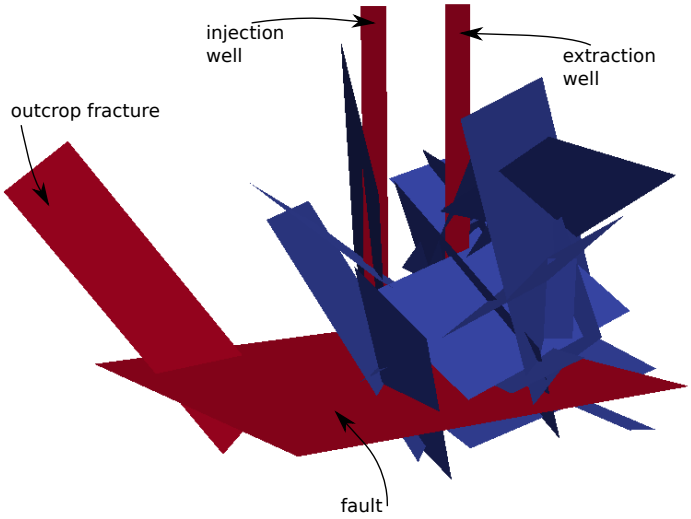

Figure 4: Test P_{uq}, geometry of the DFN

and 60 traces, see Figure 4. Two vertical fractures represent a bore-hole, which injects a pollutant in the network, and an extraction well. The fault connects the network to a nearby fracture presenting an outcrop, which may be, therefore, a carrier for a dangerous pollutant leakage. The geometry of the considered network is not based on realistic data, but is generated in order to display some of the complexities typical of networks of interest in practical applications. The network has indeed a multi-scale nature, with trace length spanning approximately three orders of magnitude and also shows some geometrical complexities, such as angles between intersecting fractures as small as few degrees, and very close and almost parallel traces in the same fracture.

We consider the phenomenon of the transport of the pollutant from the injection well into the DFN, and the effect of a random transmissivity field on this process. The quantity of interest for the present investigation, denoted by Φ, is the integral mean of the concentration of the passive pollutant at the outcrop after a fixed time period ($T = 15$ time units). Recalling that the concentration is here seen as a random variable $\mathcal{C}(t, \mathbf{x}, \omega)$ for all $t, \mathbf{x}$, we set

$$\Phi(\omega) = \int_{\Gamma_{\text{oc}}} \mathcal{C}(T, \mathbf{x}, \omega) \mathrm{d}\Gamma,$$

being Γ_{oc} the top edge of the outcrop fracture.

The transmissivity of the injection and extraction wells (F_1 and F_2), of the fault (F_3) and of the outcrop (F_4) is deterministic and set to $K_{1,2} = 1$ and $K_{3,4} = 0.5$. The transmissivity of fractures F_i, $i = 5, \ldots, 24$ is obtained along the lines of Section 6 as follows. We consider the stochastic field $K(\mathbf{x}, \omega)$ as a

function of the distance x from the fault plane, so that in (13) and subsequent equations we have $\mathbf{x} = x \in \mathbb{R}$. We choose $D = [0, 1]$ and consider an auto-covariance function given by

$$C_\kappa(x, z) = \mathrm{e}^{-\frac{|x-z|^2}{\gamma^2}}, \qquad x, z \in D\ , \tag{17}$$

being the parameter γ a measure of correlation length. We remark that other choices are possible for the auto-covariance function, such as for example functions from the Matérn family [46]. Once the truncated Karhunen-Loéve expansion $\kappa_N(x, \omega)$ is obtained as in (14), the transmissivity $K_{i,N}$ is obtained as $K_{i,N} = 2^{\kappa_N(x_i,\omega)}$, for a chosen stochastic dimension N, where x_i is the distance of the center of mass of F_i from the fault plane. Concerning the choice of γ, in order to show the viability of the proposed approach in the broadest range of situations, a small value of $\gamma = 0.125$ and a larger value of $\gamma = 0.75$ are used in the following simulations, whereas stochastic dimensions $N = 1, 2, 4$ are considered. The values obtained for the transmissivity spans therefore several orders of magnitude; the robustness of the approach in dealing with a broad range of values for the transmissivity has been investigated in [28]. The random variables Y_n in (14) are assumed to be normally distributed; consequently, we used KPN nodes for the univariate quadrature formulas and sparse grids have been generated using the `sparse grid toolkit` [47, 48] for the higher stochastic dimensions. The KPN nodes are nested and five levels of refinement for quadrature are attainable adding nodes to the previous level quadrature mesh: starting from the coarsest grid (level 0, consisting of only one node), the total number of nodes for each level is reported in Table 1. The number of nodes reported in the table and corresponding to stochastic dimensions $N > 1$ are obtained with sparse grids, instead of with a full tensorization of the univariate formula, as anticipated at the end of Section 6. We remark that increasing the number of nodes of the stochastic collocation, i.e. increasing the level of refinement, the accuracy of the quadrature formulas increases; on the other hand, increasing the stochastic dimension N corresponds to a better representation of the model, as a larger number of terms of the Karhunen-Loéve expansion is kept.

For each realization of the random transmissivity field, the Darcy velocity β in the DFN is computed by means of the optimization approach [13, 28], prescribing a fixed inflow through the top edge of the injection well and a zero hydraulic head condition at the top edge of the extraction well and of the outcrop-fracture, all other fracture edges being insulated.

Mass conservation properties of the computed velocity field β are shown by means of two error indicators, expressing the relative flux mismatch per

Table 1: Kronrod-Patterson-Normal grid nodes for the sparse grids

Level	$N = 1$	$N = 2$	$N = 4$
0	1	1	1
1	3	5	9
2	9	21	57
3	19	65	273
4	35	173	1097

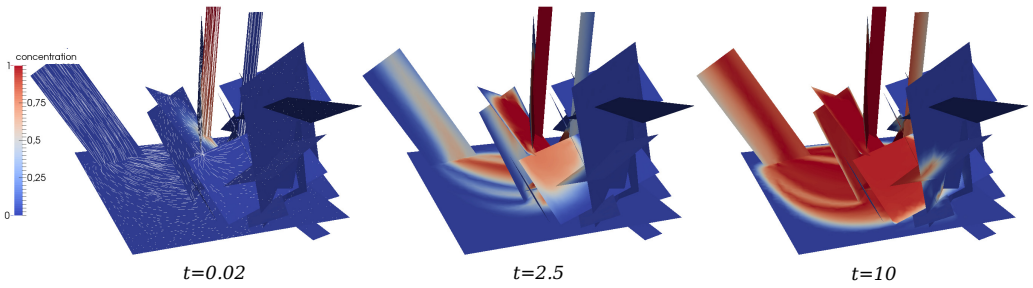

Figure 5: Solution of the DFN for problem P_{uq} at selected time-frames. Velocity field is shown in the leftmost picture: lines are directed as the velocity field and line lengths are proportional to the velocity magnitude

trace length and the relative global flux unbalance, defined respectively as:

$$\Delta_{\text{flux}} = \left(\sum_{m=1}^{M} \left\| \hat{u}_i^m + \hat{u}_j^m - \hat{\alpha} \left(h_{i|_{S_m}} + h_{j|_{S_m}} \right) \right\|^2 \right)^{\frac{1}{2}} (\bar{\chi} L)^{-1},$$

$$\Delta_{\text{cons}} = \left| \sum_{i=1}^{3} \sum_{S_m \in \mathcal{S}_i} \int_{S_m} (\hat{u}_i^m - \hat{\alpha} h_{i|_{S_m}}) \right| (\bar{\chi})^{-1},$$

in which $\hat{u}_i^m$ is the discrete control variable for trace S_m on fracture F_i for the stationary Darcy velocity problem, L is the cumulative trace length, and $\bar{\chi}$ denotes the average flux through the network:

$$\bar{\chi} = \frac{1}{2} \left(\sum_{i=1}^{3} | \sum_{S_m \in \mathcal{S}_i} \int_{S_m} (\hat{u}_i^m - \alpha h_{i|_{S_m}}) | \right).$$

The first sum in the definitions of Δ_{cons} and $\bar{\chi}$ is limited to fractures with a non-insulated portion of the boundary. The error indicators are computed for 2×10^3 randomly chosen simulations, each corresponding to a different realization of the random variables. The average value of Δ_{flux} for the considered set of simulations is 1.86×10^{-4} with a variance of 7.18×10^{-10}, whereas the average value for Δ_{cons} is 1.00×10^{-4} with a variance of 6.30×10^{-10}. These results confirm a good accuracy in the resolution of the initial Darcy problem.

Then, the time-dependent advection-diffusion problem is solved with the approach discussed in the present work, to compute pollutant concentration $\mathcal{C}$. Boundary conditions in this case are a unitary Dirichlet condition on the top edge of the injection well and a vanishing diffusive flow $\mu_i \frac{\partial \mathcal{C}_i}{\partial n} = 0$ at all other fracture edges. At time $t = 0$ there is absence of pollutant in the DFN. Simulations are performed using a mesh parameter $\delta = 10^{-3}$ resulting in about 8600 DOFs. Diffusivity parameters μ_i are taken all constant and equal to 10^{-7} for all $i = 1, \ldots, I$; the Péclet number of the problem is in the order of 10^7 and the mesh Péclet numbers span the range $10^3 - 10^5$.

In Figure 5 we show, as an example, the results obtained with one (time-dependent) realization of the problem in the case $\gamma = 0.125$. The picture reports the solution at three different time-frames, with colours proportional to the concentration of the pollutant in the DFN at the corresponding time. On the leftmost image, relative to the solution at $t = 0.02$ (corresponding to two time steps), the velocity field is also shown by means of lines directed as the velocity vectors in each point, and with length proportional to the velocity magnitude. It is possible to see how, at increasing time, the pollutant is diffused into the DFN, and reaches both the extraction well and the outcrop.

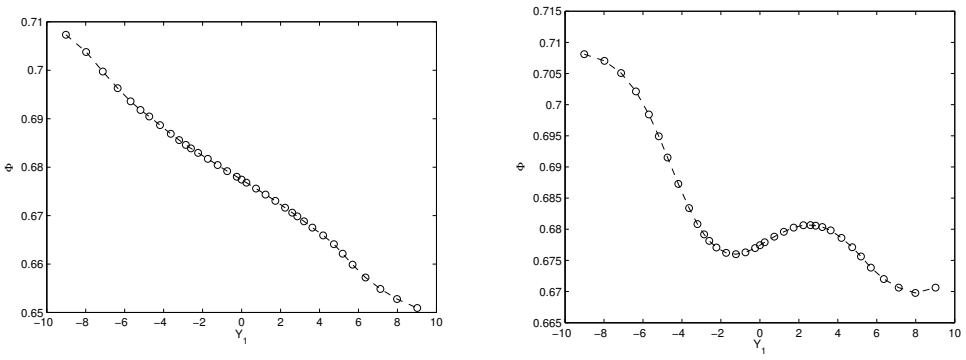

Figure 6: Plot of Φ versus the random parameter for $N = 1$; $\gamma = 0.125$ (left) and $\gamma = 0.75$ (right).

		$\gamma = 0.125$		$\gamma = 0.75$	
		$\mathbb{E}(\Phi)$	$\sigma^2(\Phi)$	$\mathbb{E}(\Phi)$	$\sigma^2(\Phi)$
Stochastic Collocation	$N = 1$	6.7740e-1	6.2248e-6	6.7769e-1	1.8029e-6
	$N = 2$	6.7670e-1	3.7730e-4	6.7710e-1	1.1967e-4
	$N = 4$	6.7655e-1	4.0343e-4	6.7709e-1	1.3376e-4
Monte Carlo Method	$N = 4$	6.7625e-1	4.0816e-4	6.7711e-1	1.4195e-4

Table 2: Computed Stochastic moments

The effect of the random transmissivity field on Φ is shown in Figure 6 for the two values of γ on the finest grid (level 4) in the case $N = 1$, i.e. corresponding to 35 different realizations of the transmissivity field (see Table 1). It can be noticed that Φ is significantly affected by the variation of the random variable Y_1, in a different manner for the two values of the parameter γ.

We now aim at measuring the convergence behaviour in the approximation of the mean value and of the variance of Φ for an increasing number of nodes in the stochastic grids. This analysis is performed taking, for each fixed stochastic dimension N, as reference solution the mean value and the variance of Φ computed on the finest stochastic grid (level 4), and measuring the relative error between the approximations of $\mathbb{E}(\Phi)$ and $\sigma^2(\Phi)$ computed on the coarser grids (levels 0 to 3) and the reference solution. Results are reported in Figure 7 for $\gamma = 0.125$ and in Figure 8 for $\gamma = 0.75$, for the three stochastic dimensions $N = 1, 2, 4$; in the same figure, we report as a comparison the results obtained for $N = 4$ with Monte Carlo method. The reference solutions obtained in all cases are reported in Table 2. Figures 7 and 8 highlight that, with the collocation approach, errors decay at a fast rate. A degradation of the convergence trend can be observed for increas-

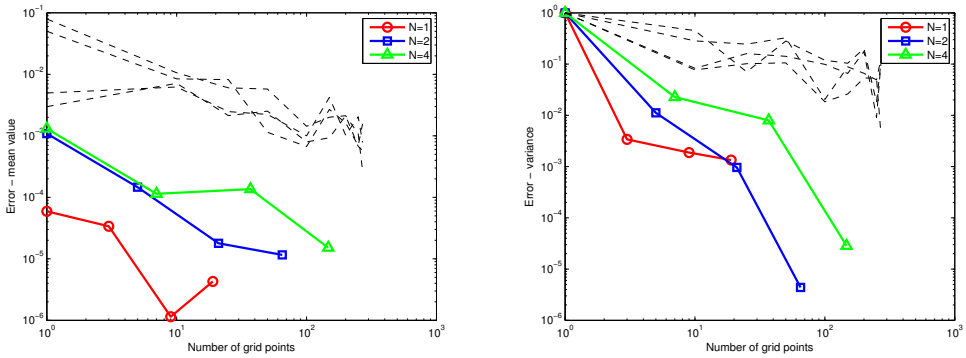

Figure 7: Convergence of the mean value (left) and variance (right) w.r.t. number of collocation nodes, dimensions $N = 1, 2, 4$, $\gamma = 0.125$. Monte Carlo simulations in dashed black lines.

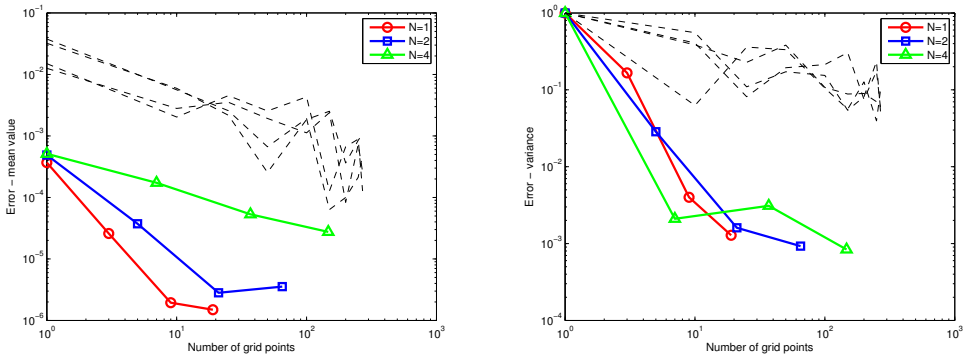

Figure 8: Convergence of the mean value (left) and variance (right) w.r.t. number of collocation nodes, dimensions $N = 1, 2, 4$, $\gamma = 0.75$. Monte Carlo simulations in dashed black lines.

ing stochastic dimensions, which is the well-known *curse of dimensionality* phenomenon (see, e.g., [39]). Comparing the errors obtained with the collocation approach to those relative to Monte Carlo simulations, it appears that the collocation strategy allows to measure the response of the model to the randomness of the data in a very effective way, thus providing reliable results without requiring a huge number of costly simulations. This is of paramount importance for such applications as the dispersion of pollutants in the subsoil, in which safety is a key aspect. Finally, note in both the cases depicted in Figures 7 and 8, the very fast decay of the errors obtained in the computation of the variance with the stochastic collocation approach, compared with those obtained with Monte Carlo method.

8. Conclusions

An optimization-based approach has been presented and numerically tested for the solution of time-dependent advection-diffusion problems in realistic DFNs. The main advantages of the method lie in the possibility of handling non-conforming meshes at the interfaces (i.e., intersections between fractures) and in a naturally parallel implementation, as demonstrated in previous works where similar methods were used for stationary diffusion problems. The method is coupled to modern uncertainty quantification techniques to measure the effect of a random transmissivity field on the dispersion of a pollutant, combining, for the first time to the best of our knowledge, uncertainty quantification strategies to time-dependent solutions in complex DFNs. Results show a fast decay of the errors for the estimated mean value and variance of a relevant quantity of interest. Given the high cost of each DFN simulation, these results appear very promising for practical applications aiming at taking into account the probabilistic nature of input data in underground flow simulations.

Acknowledgments

This work has been partially supported by the Italian Miur through PRIN research grant 2012HBLYE4_001 and by INdAM-GNCS through projects "Tecniche numeriche innovative per la simulazione di flussi in mezzi geologici poro-fratturati" and "Finanziamento GNCS Giovani Ricercatori 2015". Computational resources were partially provided by HPC@POLITO computational facility of Politecnico di Torino (http://hpc.polito.it).

References

[1] M. C. Cacas, E. Ledoux, G. de Marsily, B. Tillie, A. Barbreau, E. Durand, B. Feuga, P. Peaudecerf, Modeling fracture flow with a stochastic discrete fracture network: calibration and validation: 1. the flow model, Water Resour. Res. 26 (1990) 479–489. doi:10.1029/WR026i003p00479.

[2] A. W. Nordqvist, Y. W. Tsang, C. F. Tsang, B. Dverstop, J. Andersson, A variable aperture fracture network model for flow and transport in fractured rocks, Water Resource Res. 28 (1992) 1703–1713. doi:10.1029/92WR00216.

[3] W. S. Dershowitz, C. Fidelibus, Derivation of equivalent pipe networks analogues for three-dimensional discrete fracture networks by the boundary element method, Water Resource Res. 35 (1999) 2685–2691. doi:10.1029/1999WR900118.

[4] J. R. D. Dreuzy, P. Davy, O. Bour, Hydraulic properties of two-dimensional random fracture networks following a power law length distribution: 2., permeability of networks based on log-normal distribution of apertures, Water Resour. Res. 37 (8) (2001) 2079–2095. doi:10.1029/2001WR900010.

[5] C. Fidelibus, V. Lenti, The propagation of grout in pipe networks, Computers & Geosciences 45 (2012) 331 – 336.

[6] C. Fidelibus, The 2D hydro-mechanically coupled response of a rock mass with fractures via a mixed BEM-FEM technique, International Journal for Numerical and Analytical Methods in Geomechanics 31 (11) (2007) 1329–1348.

[7] V. Lenti, C. Fidelibus, A BEM solution of steady-state flow problems in discrete fracture networks with minimization of core storage, Computers & Geosciences 29 (9) (2003) 1183 – 1190. doi:10.1016/S0098-3004(03)00140-7.

[8] S. P. Neuman, Trends, prospects and challenges in quantifying flow and transport through fractured rocks, Hydrogeol. J. 13 (1) (2005) 124–147.

[9] G. Pichot, J. Erhel, J. de Dreuzy, A generalized mixed hybrid mortar method for solving flow in stochastic discrete fracture networks, SIAM Journal on scientific computing 34 (2012) B86 – B105. doi:10.1137/100804383.

[10] J. Hyman, C. Gable, S. Painter, N. Makedonska, Conforming Delaunay triangulation of stochastically generated three dimensional discrete fracture networks: A feature rejection algorithm for meshing strategy, SIAM Journal on Scientific Computing 36 (2014) A1871–A1894. doi:10.1137/130942541.

[11] H. Mustapha, K. Mustapha, A new approach to simulating flow in discrete fracture networks with an optimized mesh, SIAM J. Sci. Comput. 29 (4) (2007) 1439–1459. doi:10.1137/060653482.

[12] A. Fumagalli, A. Scotti, A numerical method for two-phase flow in fractured porous media with non-matching grids, Advances in Water Resources 62 (2013) 454 – 464. doi:10.1016/j.advwatres.2013.04.001.

[13] S. Berrone, S. Pieraccini, S. Scialò, A PDE-constrained optimization formulation for discrete fracture network flows, SIAM J. Sci. Comput. 35 (2) (2013) B487–B510. doi:10.1137/120865884.

[14] M. Benedetto, S. Berrone, S. Scialò, A globally conforming method for solving flow in discrete fracture networks using the virtual element method, Finite Elem. Anal. Des. 109 (2016) 23–36. doi:10.1016/j.finel.2015.10.003.

[15] M. Benedetto, S. Berrone, A. Borio, S. Pieraccini, S. Scialò, A hybrid mortar virtual element method for discrete fracture network simulations, J. Comput. Phys. 306 (2016) 148–166. doi:10.1016/j.jcp.2015.11.034.

[16] N. Makedonska, S. L. Painter, Q. M. Bui, C. W. Gable, S. Karra, Particle tracking approach for transport in three-dimensional discrete fracture networks, Computational Geosciences 19 (5) (2015) 1123–1137. doi:10.1007/s10596-015-9525-4.

[17] J. D. Hyman, S. Karra, N. Makedonska, C. W. Gable, S. L. Painter, H. S. Viswanathan, dfnWorks: A discrete fracture network framework for modeling subsurface flow and transport, Computers & Geosciences 84 (2015) 10 – 19. doi:10.1016/j.cageo.2015.08.001.

[18] B. Nœtinger, A quasi steady state method for solving transient Darcy flow in complex 3D fractured networks accounting for matrix to fracture flow, Journal of Computational Physics 283 (2015) 205 – 223. doi:10.1016/j.jcp.2014.11.038.

[19] B. Nœtinger, N. Jarrige, A quasi steady state method for solving transient Darcy flow in complex 3D fractured networks, Journal of Computational Physics 231 (1) (2012) 23 – 38. doi:10.1016/j.jcp.2011.08.015.

[20] B. Nœtinger, D. Roubinet, A. Russian, T. Le Borgne, F. Delay, M. Dentz, J.-R. de Dreuzy, P. Gouze, Random walk methods for modeling hydrodynamic transport in porous and fractured media from pore to reservoir scale, Transport in Porous Media (2016) 1–41doi:10.1007/s11242-016-0693-z.

[21] S. Berrone, S. Pieraccini, S. Scialò, On simulations of discrete fracture network flows with an optimization-based extended finite element method, SIAM J. Sci. Comput. 35 (2) (2013) A908–A935. doi:10.1137/120882883.

[22] S. Berrone, S. Pieraccini, S. Scialò, An optimization approach for large scale simulations of discrete fracture network flows, J. Comput. Phys. 256 (2014) 838–853. doi:10.1016/j.jcp.2013.09.028.

[23] M. Benedetto, S. Berrone, S. Pieraccini, S. Scialò, The virtual element method for discrete fracture network simulations, Comput. Methods Appl. Mech. Engrg. 280 (0) (2014) 135 – 156. doi:10.1016/j.cma.2014.07.016.

[24] S. Berrone, C. Fidelibus, S. Pieraccini, S. Scialò, Simulation of the steady-state flow in discrete fracture networks with non-conforming meshes and extended finite elements, Rock Mechanics and Rock Engineering 47 (6) (2014) 2171–2182. doi:10.1007/s00603-013-0513-5.

[25] S. Berrone, C. Canuto, S. Pieraccini, S. Scialò, Uncertainty quantification in discrete fracture network models: stochastic fracture transmissivity, Comput. Math. Appl. 70 (4) (2015) 603–623. doi:10.1016/j.camwa.2015.05.013.

[26] S. Berrone, S. Pieraccini, S. Scialò, F. Vicini, A parallel solver for large scale DFN flow simulations, SIAM J. Sci. Comput. 37 (3) (2015) C285–C306. doi:10.1137/140984014.

[27] S. Berrone, A. Borio, S. Scialò, A posteriori error estimate for a PDE-constrained optimization formulation for the flow in DFNs, SIAM J. Numer. Anal. 54 (1) (2016) 242–261. doi:10.1137/15M1014760.

[28] S. Berrone, S. Pieraccini, S. Scialò, Towards effective flow simulations in realistic discrete fracture networks, J. Comput. Phys. 310 (2016) 181–201. doi:10.1016/j.jcp.2016.01.009.

[29] M. Vohralík, J. Maryška, O. Severýn, Mixed and nonconforming finite element methods on a system of polygons, Applied Numerical Mathematics 51 (2007) 176–193.

[30] L. Formaggia, A. Fumagalli, A. Scotti, P. Ruffo, A reduced model for Darcy's problem in networks of fractures, ESAIM: Mathematical Modelling and Numerical Analysis 48 (2014) 1089–1116. doi:0.1051/m2an/2013132.

[31] V. Martin, J. Jaffré, J. E. Roberts, Modeling fractures and barriers as interfaces for flow in porous media, SIAM Journal on Scientific Computing 26 (5) (2005) 1667–1691. doi:10.1137/S1064827503429363.

[32] M. Benedetto, S. Berrone, A. Borio, S. Pieraccini, S. Scialò, Order preserving SUPG stabilization for the virtual element formulation of advection-diffusion problems, Comput. Methods Appl. Mech. Engrg. 311 (2016) 18–40. doi:10.1016/j.cma.2016.07.043.

[33] L. P. Franca, S. L. Frey, T. J. Hughes, Stabilized finite element methods: I. Application to the advective-diffusive model, Computer Methods in Applied Mechanics and Engineering 95 (2) (1992) 253 – 276. doi:10.1016/0045-7825(92)90143-8.

[34] I. Harari, T. Hughes, What are c and h?: Inequalities for the analysis and design of finite element methods, Computer Methods in Applied Mechanics and Engineering 97 (2) (1992) 157–192. doi:10.1016/0045-7825(92)90162-D.

[35] S. Berrone, M. Marro, Space-time adaptive simulations for unsteady Navier-Stokes problems, Computers & Fluids 38 (6) (2009) 1132 – 1144. doi:10.1016/j.compfluid.2008.11.004.

[36] O. P. Le Maître, O. M. Knio, Spectral methods for uncertainty quantification. With applications to computational fluid dynamics, Scientific Computation, Springer, New York, 2010.

[37] D. Xiu, J. S. Hesthaven, High-order collocation methods for differential equations with random inputs, SIAM J. Sci. Comput. 27 (3) (2005) 1118–1139 (electronic).

[38] I. Babuška, F. Nobile, R. Tempone, A stochastic collocation method for elliptic partial differential equations with random input data, SIAM J. Numer. Anal. 45 (3) (2007) 1005–1034.

[39] F. Nobile, R. Tempone, C. G. Webster, A sparse grid stochastic collocation method for partial differential equations with random input data, SIAM J. Numer. Anal. 46 (5) (2008) 2309–2345.

[40] S. Smolyak, Quadrature and interpolation formulas for tensor products of certain classes of functions,, Dokl. Akad. Nauk 4 (1963) 240–243.

[41] H.-J. Bungartz, M. Griebel, Sparse grids, Acta Numer. 13 (2004) 147–269.

[42] T. N. L. Patterson, The optimum addition of points to quadrature formulae, Math. Comp. 22 (1968) 847–856.

[43] L. N. Trefethen, Is Gauss quadrature better than Clenshaw-Curtis?, SIAM Rev. 50 (1) (2008) 67–87.

[44] A. Genz, B. D. Keister, Fully symmetric interpolatory rules for multiple integrals over infinite regions with Gaussian weight, J. Comput. Appl. Math. 71 (1996) 299–309.

[45] T.-P. Fries, T. Belytschko, The extended/generalized finite element method: an overview of the method and its applications, Internat. J. Numer. Methods Engrg. 84 (3) (2010) 253–304. doi:10.1002/nme.2914.

[46] C. E. Rasmussen, C. K. I. Williams, Gaussian Processes for Machine Learning, The MIT Press, 2006.

[47] F. Nobile, L. Tamellini, Sparse grids Matlab kit, http://csqi.epfl.ch/ (2014).

[48] J. Bäck, F. Nobile, L. Tamellini, R. Tempone, Stochastic spectral Galerkin and collocation methods for PDEs with random coefficients: a numerical comparison, in: J. S. Hesthaven, E. Ronquist (Eds.), Spectral and High Order Methods for Partial Differential Equations, Lecture notes in computational science and engineering 76, Springer, 2011, pp. 43–62.